Soil cation storage as a key control on the timescales of carbon dioxide removal through enhanced weathering

Authors: Y. Kanzaki[1], N.J. Planavsky[2,3], S. Zhang[4], J. Jordan[5], C.T. Reinhard[1*]

Affiliations:

[1]School of Earth and Atmospheric Sciences, Georgia Institute of Technology, Atlanta, GA, USA.
[2]Department of Earth and Planetary Sciences, Yale University, New Haven, CT, USA.
[3]Yale Center for Natural Carbon Capture, New Haven, CT, USA.
[4]Department of Oceanography, Texas A&M, College Station, TX, USA.
[5]Porecast Research, LLC, Lawrence, KS, USA.

[*]corresponding author: chris.reinhard@eas.gatech.edu

Key Points:

- Cation storage in soils can temporarily undo the carbon dioxide removal that occurs during the enhanced weathering process.
- Lags in carbon removal after carbonate or silicate weathering can vary from years to many decades.
- Carbon removal lags should be quantified in enhanced weathering deployments through rigorous validation of models with real-world data.

Abstract: Significant interest and capital are currently being channeled into techniques for durable carbon dioxide removal (CDR) from Earth's atmosphere. A particular class of these approaches — referred to as enhanced weathering (EW) — seeks to modify the surface alkalinity budget to durably store CO_2 as dissolved inorganic carbon species. Here, we use SCEPTER — a reaction-transport code designed to simulate EW in managed lands — to evaluate the throughput and storage timescales of anthropogenic alkalinity in agricultural soils. Through a series of alkalinity flux simulations, we explore the main controls on cation storage and export from surface soils in key U.S. agricultural regions. We find that lag times between alkalinity modification and climate-relevant CDR can span anywhere from years to many decades, with background soil cation exchange capacity, agronomic target pH, and fluid infiltration all impacting the timescales of CDR relative to the timing of alkalinity input. There may be scope for optimization of weathering-driven alkalinity transport through variation in land management practice. However, there are tradeoffs with total CDR, optimal nutrient use efficiencies, and soil nitrous oxide (N_2O) fluxes that complicate attempts to perform robust time-resolved analysis of the net radiative impacts of CDR through EW in agricultural systems. Although CDR lag times will be more of an issue in some regions than others, these results have significant implications for the technoeconomics of EW and the integration of EW into voluntary carbon markets, as there may often be a large temporal disconnect between deployment of EW and climate-relevant CDR.

1. Introduction

Efforts to achieve key milestones aimed at limiting the extent of anthropogenic climate disruption in the coming century will very likely require significant amounts of net carbon dioxide removal (CDR) from Earth's atmosphere. Specifically, even optimistic scenarios for decarbonization of energy systems, transport, and industry in the coming decades still require roughly 1-10 gigatons of carbon dioxide ($GtCO_2$, 10^9 tons of CO_2) to be removed from the atmosphere each year by the end of the century to achieve net carbon neutrality [*IPCC*, 2018; *Rogelj et al.*, 2018]. The current supply of durable CDR — defined as carbon removal that is durable on timescale similar to or greater than the residence time of CO_2 in the atmosphere (~100 years) — is many orders of magnitude below this [*Smith et al.*, 2023]. There is thus strong impetus for rapid scaling of promising durable CDR approaches, and significant amounts of private and public funding flowing into efforts to develop the basic science underlying durable CDR pathways and bring them to scale.

Enhanced weathering (EW) is one particularly promising geochemical approach toward durable CDR. Enhanced weathering involves adding fine-grained cation-rich rock feedstocks (typically basalt, olivine, wollastonite, or steel slag) to soils, where they dissolve in the presence of elevated soil CO_2 to yield bicarbonate (HCO_3^-). This bicarbonate can in principle be transported by river/stream systems to the oceans, where much of it will remain stored on timescales on the order of 10^4 years [*Kanzaki et al.*, 2023b; *Lord et al.*, 2015; *Renforth and Henderson*, 2017]. Carbonate (limestone) weathering – currently in widespread use as an agricultural practice for soil pH management – can also lead to alkalinity export and CDR, although the efficiency and dynamics of this process are dependent in part on the pH at which weathering occurs [*Hamilton et al.*, 2007; *Oh and Raymond*, 2006]. Because it has the potential to leverage extensive existing agricultural infrastructure, requires relatively little energy beyond that required to transport feedstock, and may have a range of agronomic and socioeconomic co-benefits, EW has attracted considerable interest as a durable CDR pathway that has the potential to scale rapidly in a relatively cost-effective way [*Baek et al.*, 2023; *Beerling et al.*, 2020; *Beerling et al.*, 2018; *Calabrese et al.*, 2022].

However, there is a range of possible fates for cations released from EW feedstocks, including calcium carbonate or secondary clay mineral formation in terrestrial settings [*Bluth and Kump*, 1994; *Lal*, 2007], re-equilibration of the carbonic acid system in rivers and streams [*Harrington et al.*, 2023; *Knapp and Tipper*, 2022; *Zhang et al.*, 2022], and storage of cations on exchange sites within soils and in the lower critical zone [*Appelo*, 1994; *Bolt et al.*, 1976; *Spencer*, 1954]. In the case of (permanent) secondary mineral formation and carbonic acid system re-equilibration CO_2 is released back to the atmosphere, undoing the initial CDR. In the case of cation storage CDR is instead delayed for an exchange timescale, as cation storage in soils is ultimately reversible and released cations will be charge balanced by HCO_3^- production upon release from the soil exchange complex (an exception to this may be EW using limestone as a feedstock, which could in some cases result in transient net CO_2 release rather than delayed CO_2 removal).

Methods are currently being developed for tracking the initial release of cations from EW feedstocks [e.g., *Reershemius et al.*, 2023]. These approaches can provide an estimate of the "CDR potential" that will eventually emerge assuming no downstream cation removal or CO_2 degassing. However, the timescales over which this CDR potential will be realized are poorly known. This is critical for the technoeconomics of EW, because a ton of carbon removed immediately has more value than a ton of carbon removed in the future [e.g., *Fearnside et al.*, 2000; *Groom and Venmas*,

2023; *Richards*, 1997; *van Kooten et al.*, 2021]. As a result, offset purchase contracts using EW as a pathway must either accurately discount lagged carbon removal *ex-ante* or have *ex-post* guardrails for empirically verifying cation fluxes through the system over time. In either case, timescales of cation lag that are sufficiently long could potentially render EW projects unworkable for some voluntary carbon markets as currently structured.

Here, we use a reaction-transport code [*Kanzaki et al.*, 2023a; *Kanzaki et al.*, 2022] designed to simulate enhanced weathering (EW) in managed lands to evaluate the throughput and storage timescales of anthropogenic alkalinity in agricultural soils. Through a series of idealized alkalinity flux simulations, we explore the main controls on cation storage and export from surface soils in key U.S. agricultural regions. We find that carbon removal lags induced by transient cation storage in soils can range from years to many decades — varying significantly across key agricultural regions of the U.S. – and suggest that carbon removal lags due to cation storage need to be considered in future EW research and deployment efforts. Lastly, we discuss the implications of these results for deployment of EW on carbon markets and suggest potential strategies through which background soil characteristics and deployment practice can both be leveraged to shorten carbon removal lags.

2. Materials and Methods

2.1 A gridded dataset for simulated alkalinity modification in U.S. agricultural regions

We focus here on key agricultural regions of the coterminous United States, basing our analysis on areas with a cropland fraction greater than 10% and gridded at a resolution of 1ºx1º. As boundary conditions for the initialization and spin-up of our reaction-transport code we use a series of gridded data products for runoff, mean annual air temperature (MAT), soil moisture, aboveground net primary productivity (NPP), soil organic matter (SOM), fertilization rate, topsoil pH, soil cation exchange capacity (CEC), and soil base saturation (**Fig. 1**). Observational data are derived from the sources shown in **Table 1**. Soil pCO_2 was calculated as a function of net primary production (NPP) and temperature according to the method of [*Gwiazda and Broecker*, 1994] adapted and modified by [*Goddéris et al.*, 2010], [*Gaillardet et al.*, 2019], and [*Zeng et al.*, 2022].

The reaction-transport model used here is designed to track feedstock-specific alkalinity release and cation/carbon biogeochemistry in managed soils [*Kanzaki et al.*, 2023a; *Kanzaki et al.*, 2022]. We adopt a model configuration that is essentially the same as that described in [*Kanzaki et al.*, 2023a], which consists of two solid species (bulk soil phase plus soil organic matter), one gaseous species (CO_2), and an inclusive range of aqueous species for evaluating charge balance and soil acid-base balance [*Kanzaki et al.*, 2022]. We use four tuning parameters to initialize the soil column in each grid cell: (1) an aggregate cation exchange parameter ($K_{H/Na}$); (2) a dissolved Ca^{2+} concentration at the upper boundary of the soil column, which is a convenient way of representing historical agricultural liming; (3) an input flux of organic carbon (OC) to the soil; and (4) a time constant for organic carbon turnover (**Fig. 2**). These parameters are tuned to match the observed values for soil pH, base saturation, soil organic matter content, and soil pCO_2 (**Fig. 1**), with the soil column in each grid cell being spun up for 10^5 years to achieve steady state prior to alkalinity modification.

Following spinup and initialization, we conduct alkalinity modification experiments in which CaO is added as a source of alkalinity to the system. CaO is chosen as a feedstock because the dissolution and alkalinity release are extremely rapid – the approach is designed to remove the time-dependent uncertainty in dissolution rates associated with dissolution of less labile (but more readily deployed) feedstocks such as basalt or olivine, and to isolate the effects of cation exchange on the timescales of CDR. In the simulations shown here, feedstock is added continuously and mixed homogeneously down to a depth of 25cm. Feedstock addition rate is iteratively tuned to reach a specified agronomic target pH ($pH_t = 7.0$) after one year of application. In-silico agronomic soil pH is calculated by the method described in [*Kanzaki et al.*, 2023a] as the bulk phase pH value of simulated soil in 1 mM $CaCl_2$ solution, equilibrated at a 1:2.5 (g/cm^3) soil/solution ratio. The model domain for all simulations is 50 cm, which for our purposes is expected to yield a conservative (i.e., lower-bound) estimate of cation travel times through the soil column.

2.2 CDR calculation methods

We evaluate CDR over time in the simulated soil column using three metrics, each of which is designed to correspond to a distinct set of techniques for measurement, reporting, and verification (MRV) of CDR in enhanced weathering deployments. The first is scaled to the fraction of feedstock that dissolves in the soil (CDR_{diss}):

$$\mathrm{CDR_{diss}} = \frac{\sum_{\theta} \gamma_\theta \Delta J_\theta^{diss}}{\sum_{\theta} \gamma_\theta \Delta J_\theta^{feed}} \quad , \tag{1}$$

where γ_θ is the molar ratio of potential CO_2 capture per unit dissolution of feedstock θ (e.g., $\gamma_{CaO} = 2$), J_θ^{feed} and J_θ^{diss} are deployment (spreading) and dissolution fluxes of feedstock θ (mol m^{-2} y^{-1}), respectively, and Δ denotes the flux difference between scenarios with and without feedstock deployment. Mechanistically, this metric corresponds to time-integrated solid-phase approaches for tracking on-field rates of CDR [*Beerling et al.*, 2024; *Kantola et al.*, 2023; *Reershemius et al.*, 2023; *Reershemius and Suhrhoff*, 2023]. In short, these techniques rely on measuring mobile cations and immobile elements in soil before and after feedstock application and using these measurements to estimate loss of base cations from applied feedstock. It is important to emphasize that these techniques do not track CDR directly, and instead provide an estimate of "potential" CDR that will emerge over time once the base cations have been charge balanced by alkalinity production [*Reershemius et al.*, 2023].

The second CDR metric employed here is scaled to the reduction of gaseous CO_2 exchange between the soil column and the atmosphere (CDR_{diff}):

$$\mathrm{CDR_{diff}} = \frac{\Delta J_{CO_2} - \Delta J_{SOC}}{\sum_{\theta} \gamma_\theta \Delta J_\theta^{feed}} \quad , \tag{2}$$

where γ_θ, J_θ^{feed}, and Δ are defined as above and J_{CO2} and J_{SOC} are the soil-atmosphere flux of CO_2 (mol m^{-2} y^{-1}) and the decomposition flux (mol m^{-2} y^{-1}) of soil organic carbon (SOC), respectively. Mechanistically, this metric reflects a decrease in the flux of CO_2 from the soil column to the

atmosphere due to HCO_3^- production in the soil, and could in principle be measured through CO_2 gas fluxes from treated and control soils via eddy flux towers [*Baldocchi*, 2003], flux chambers[*Pumpanen et al.*, 2004], or gas-phase CO_2 sensors[*Yasuda et al.*, 2007]. In contrast to the solid-phase metric shown by Eq. (1), this metric tracks CDR directly and reflects additional HCO_3^- production (and a corresponding reduction of the soil-atmosphere CO_2 flux) due to soil management.

Lastly, we can scale CDR efficiency to the increase in advective fluxes of aqueous dissolved inorganic carbon species through the soil column (CDR_{adv}):

$$\mathrm{CDR_{adv}} = \frac{\Delta J_{DIC} - \Delta J_{SIC}}{\sum_{\theta} \gamma_{\theta} \Delta J_{\theta}^{feed}} \quad , \tag{3}$$

Where γ_θ, J_θ^{feed}, J_{SIC}, and Δ are defined as above and J_{DIC} represents the flux (mol m^{-2} y^{-1}) of total dissolved inorganic carbon (i.e., aqueous CO_2, HCO_3^-, and CO_3^{2-}) advected out of soil column. Mechanistically, this metric reflects additional HCO_3^- production and advection out of the system due to feedstock application and could in principle be measured by lysimeter techniques at the field scale [*Weihermüller et al.*, 2007], point-collected dissolved solute measurements at the catchment scale [*Larkin et al.*, 2022] , or possibly at larger scales through measurements of solute composition in stream/river systems. Similar to Eq. (2), this metric directly tracks net CDR in the soil column rather than gross alkalinity release.

Note that all of these metrics for CDR efficiency are referenced to the maximum potential CDR, which assumes that all base cations released from feedstock θ are instantly and completed leached upon deployment and charge-balanced only by production of bicarbonate ions. At steady state, the reduction in soil-atmosphere CO_2 flux should be equivalent to the increase in bicarbonate advection ($CDR_{diff} \sim CDR_{adv}$). In the case of negligible cation sinks (e.g., secondary carbonate or silicate mineral phases) and on arbitrarily long timescales, $CDR_{diss} \sim CDR_{diff} \sim CDR_{adv}$. However, transient cation storage could result in lag periods for which CDR_{diff} (or CDR_{adv}) < CDR_{diss}. This allows us to isolate and quantify cation storage lags through time-dependent offsets between CDR_{diss} and CDR_{diff}/CDR_{adv}.

3. Results

We first examine timescales of alkalinity release, cation exchange, and carbon removal in four representative sites across major agricultural regions in the U.S.: (1) Site 128, located in the Northern Plains region; (2) Site 311, located in the Corn Belt; (3) Site 161, located in the Southern Plains region; and (4) Site 411, located in the Southeast (**Fig. 1, 2**). As expected, alkalinity release into the system is effectively instantaneous across all sites (**Fig. 3**), with dissolution-based CDR (CDR_{diss}) matching effective CDR potential (CDR_{eff}) on a timescale of days to weeks. Again, this is by design, as our intent is to isolate exchange and transport lags from feedstock dissolution lags. However, most of the alkalinity released from feedstock is initially stored as exchangeable calcium (Ca_{exch}) and is only gradually released back into the system as an advective cation flux (Ca_{adv}) over timescales ranging from years to decades (**Fig. 3**). This causes a significant lag in carbon removal relative to alkalinity input because it is only when the exchangeable calcium is released into the advective flux and charge balanced by HCO_3^- production that CDR can occur.

Although there is often a slight offset between carbon removal based on soil-atmosphere CO_2 exchange (CDR_{diff}) and advection of new DIC (CDR_{adv}) in the first decade, they, as expected, track each other closely. These two metrics for carbon removal should be equivalent at steady state. The timescales of actual carbon removal (tracked by both CDR_{diff} and CDR_{adv}) are significantly longer than those of alkalinity release (tracked by CDR_{diss}) across all sites (**Fig. 3**). For example, for our deployment in the Corn Belt CDR_{diff} and CDR_{adv} reach only ~40% of the effective CDR potential after 10 years, with a timescale of ~50 years required to reach 80% of effective carbon removal (**Fig. 3b**). In contrast, realized CDR reaches ~80% of its potential within the first decade after deployment in the Southeast regional site (**Fig. 3d**).

Because the timescale required to achieve a particular threshold of CDR potential varies by region, we geospatially analyze carbon removal lags across key agricultural regions in the U.S. (**Fig. 4**). There are relatively few sites that show any tangible carbon removal in the first year despite instantaneous cation and alkalinity input (**Fig. 4a**), and these are generally restricted to scattered locations in the southeastern U.S. (Alabama, Georgia, and Florida; **Fig. 4e,i**). Most of the regions examined here are below 50% of effective CDR potential after 5 years, and in some regions (the Corn Belt and Great Plains) it takes well over 10 years after instantaneous cation and alkalinity input for carbon removal to occur (**Fig. 4h,l**). Considering all regions together, it takes roughly 10 years to surpass a median carbon removal efficiency of 50%, with a median CDR efficiency of 75% surpassed in ~20 years (**Fig. 5d,g**). However, median lag times vary significantly by region — for instance, in the Corn Belt median CDR lag is ~50 years to achieve 75% of CDR potential, while the same carbon removal potential is achieved in the Southeast nearly an order of magnitude more rapidly (**Fig. 5h,i**).

The magnitude of cation lag at any site clearly varies as a function of background soil characteristics. This is evident, for example, in the Southeast sites which generally show significantly shorter lag times overall as a result of very low cation exchange capacities with high water fluxes (**Fig. 1h, 4f,j, 5f,i**). At the same time, soil management strategy can also significantly impact cation lag times. For example, increasing agronomic target pH (pH_t) can result in significantly higher CDR efficiency for a given time horizon (**Fig. 6**) because of gradual cation loading on the soil exchange complex, which is more rapid at the higher alkalinity fluxes associated with higher pH_t. The impact of this can be significant – in the case of Site 411, a value of pH_t = 5.5 results in an advective CDR efficiency of ~30% after ten years, while the same CDR efficiency can be achieved in only ~2 years at pH_t = 7.0.

4. Discussion

Our results suggest that carbon dioxide removal lags induced by cation exchange in agricultural soils can be significant, and in some cases can last multiple decades, adding to a robust evidence base for the following key conclusions: (1) cation sorption in soils with low base saturation (the ratio of cations to protons in soil sorption sites) will delay climate-relevant CO_2 removal in EW deployments; (2) this lag time can be multiple years or even several decades; and (3) these lag times will vary geographically and with management practice. However, it is important to stress that although these basic conclusions are very likely robust, we do not currently have firm constraints on the uncertainty in lag times for any individual region or deployment strategy, and there is a pressing need to validate model estimates of carbon removal lag against real-world

observations. As a result, we would strongly argue that given the current state of knowledge reaction-transport models are not equipped to provide robust estimates of CDR lag for ready inclusion in carbon accounting schemes [e.g., *Balmford et al.*, 2023].

Our time lag estimates may be conservative, given that our lag estimates are based on simulations with a 50 cm vertical domain and soil thickness throughout agricultural regions of the U.S. is significantly greater than this [e.g., *Pelletier et al.*, 2016], such that the overall alkalinity input required to saturate the soil exchange complex would be larger. On the other hand, it is expected that there will be a certain length scale at which soils will become diffusionally isolated from the atmosphere. This isolation length scale will very likely vary with soil type and seasonally, which combine to drive time-dependent changes to soil moisture and fluid saturation. In addition, the apparent role of target pH in enhancing or inhibiting cation and alkalinity throughput (**Fig. 6**) could be complicated by implementation of more realistic feedstock dissolution kinetics. There is a well-known scaling between ambient soil pH and rates of feedstock dissolution [e.g., *Kump et al.*, 2000; *Snaebjörnsdóttir et al.*, 2020], such that there should be a tradeoff between more effective cation throughput when target pH is continuously maintained at a high value and less effective feedstock dissolution. This dynamic represents an important topic for future research.

An extended carbon removal lag after weathering induced by soil cation exchange has several significant implications for deployment of EW in a market framework. Most importantly, the economic value of carbon removal is time-varying, which means that EW deployments that aim to sell carbon offsets on a voluntary market should be able to accurately quantify the timing of climate-relevant CDR across timescales. One reasonable conclusion would be that suppliers of EW-based offsets on a voluntary market should be expected to either confront the technical challenge of quantifying carbon removal lags prior to deployment or the challenges to project finance associated with empirically verifying carbon removal over extended timescales prior to receiving revenue for offset production. The structure of carbon marketplaces could also be modified to account for this feature of the EW pathway. In any case, our results suggest that cation storage is ubiquitous and needs to be considered in any EW deployment.

There is significant potential scope for optimizing the efficiency of alkalinity transport through soils via both deployment siting and land management practice. For instance, our idealized deployment scheme – in particular, continuously managing soil pH at a uniform optimal agronomic value – is not optimized for cation transit through the soil column and from a land management perspective is also unlikely to be pursued in practice. Pulsed alkalinity addition followed by cation flushing with strong acid from fertilizer application may increase the efficiency of alkalinity transport in managed soils. However, one would expect lower time-integrated CDR overall, along with higher time-integrated soil N_2O fluxes [*Blanc-Betes et al.*, 2020; *Chiaravalloti et al.*, 2023; *Kantola et al.*, 2023; *Val Martin et al.*, 2023; *Wang et al.*, 2021b], in scenarios in which pH is intentionally and repeatedly lowered to enhance cation flushing. Additionally, in large-scale interpolated soil databases there are some regions that show increased pH and base cation abundance in the exchange complex at depth [e.g., *Poggio et al.*, 2021]. In some cases, these gradients may enhance local alkalinity export. In any case, there are currently large uncertainties in quantifying the tradeoffs and overall impacts of optimized alkalinity throughput on agricultural greenhouse gas budgets, and this represents a critical topic for future research.

Perhaps most importantly, our results highlight the need for more empirical constraints on cation and alkalinity throughput in managed lands. Accurate representation of the soil exchange complex in process-based models such as that explored here is challenging, and there is currently significant uncertainty in the dynamics of cation breakthrough in managed soils that are well out of steady state. Moving forward, the production of large datasets that can constrain cation fluxes and carbon removal lag times, some of which could be produced by private-sector suppliers of carbon removal through EW, would represent a major step forward in our ability to accurately quantify cation storage across a range of scenarios and deployment strategies. There is a pressing need for these data to be rigorously and transparently evaluated, and for the results to be leveraged in the development of process-based models of soil cation exchange and time-dependent charge balance dynamics.

5. Conclusions

Soil biogeochemical modeling suggests that cation exchange dynamics in agricultural soils can lead to significant lags between alkalinity input from EW feedstocks (weathering) and climate-relevant carbon dioxide removal. Lag times can vary from less than a year to many decades and will be controlled by background soil characteristics and land management practice. In some cases, carbon removal lags can be reduced through thoughtful site selection and/or optimized soil pH management. However, carbon removal lags induced by soil cation storage should be ubiquitous in the field, and EW deployments that commodify carbon removal through charge balance must take storage-induced removal lags into account. In the near-term, this will require rigorous and transparent validation of reaction-transport models against real-world observations of alkalinity throughput in managed lands.

Data Availability Statement:

All observational datasets used here are available through the references given in Table 1. The model code used here (SCEPTER-v1.0) is publicly available in [*Kanzaki et al.*, 2023a], with a tagged release archived permanently at https://doi.org/10.5281/zenodo.8078586.

Funding: NJP acknowledges funding from the Yale Center for Natural Carbon Capture (YCNCC), NJP and CTR acknowledge funding from the Grantham Foundation.

Author contributions:

Conceptualization: YK, CTR, NJP
Methodology: YK, SZ, CTR, NJP
Investigation: YK, SZ, CTR, NJP
Visualization: YK, CTR, NJP
Funding acquisition: CTR, NJP
Project administration: CTR, NJP
Supervision: CTR, NJP
Writing – original draft: CTR, YK
Writing – review & editing: YK, CTR, NJP, SZ, JJ

Competing interests: JJ is employed by Mati Carbon, A B-Corp owned by the not-for-profit organization Swaniti Initiative.

References:

Appelo, C. A. J. (1994), Cation and proton exchange, pH variations, and carbonate reactions in a freshening aquifer, *Water Resources Research*, *30*, 2793-2805.

Baek, S. H., Y. Kanzaki, J. M. Lora, N. J. Planavsky, C. T. Reinhard, and S. Zhang (2023), Impact of climate on the global capacity for enhanced rock weathering on croplands, *Earth's Future*, *11*.

Baldocchi, D. D. (2003), Assessing the eddy covariance technique for evaluating carbon dioxide exchange rates of ecosystems: past, present and future, *Global Change Biology*, *9*, 479-492.

Balmford, A., S. Keshav, F. Venmans, D. A. Coomes, B. Groom, A. Madhavapeddy, and T. Swinfield (2023), Realizing the social value of impermanent carbon credits, *Nature Climate Change*, *13*, 1172-1178.

Beerling, D. J., et al. (2024), Enhanced weathering in the US Corn Belt delivers carbon removal with agronomic benefits, *Proceedings of the National Academy of Sciences, USA*, *121*, doi:10.1073/pnas.2319436121.

Beerling, D. J., et al. (2020), Potential for large-scale CO2 removal via enhanced rock weathering with croplands, *Nature*, *583*, 242-248.

Beerling, D. J., et al. (2018), Farming with crops and rocks to address global climate, food and soil security, *Nature Plants*, *4*, 138-147.

Blanc-Betes, E., I. B. Kantola, N. Gomez-Casanovas, M. D. Hartman, W. J. Parton, A. L. Lewis, D. J. Beerling, and E. H. DeLucia (2020), In silico assessment of the potential of basalt amendments to reduce N2O emissions from bioenergy crops, *GCB Bioenergy*, *13*, 224-241.

Bluth, G. J. S., and L. R. Kump (1994), Lithologic and climatologic controls of river chemistry, *Geochimica et Cosmochimica Acta*, *58*, 2341-2359.

Bolt, G. H., M. G. M. Bruggenwert, and A. Kamphorst (1976), Adsorption of cations by soil, in *Developments in Soil Science*, edited by G. H. Bolt and M. G. M. Bruggenwert, pp. 54-90.

Calabrese, S., B. Wild, M. B. Bertagni, I. C. Bourg, C. White, F. Aburto, G. Cipolla, L. V. Noto, and A. Porporato (2022), Nano- to global-scale uncertainties in terrestrial enhanced weathering, *Environmental Science & Technology*, doi:10.1021/acs.est.2c03163.

Chiaravalloti, I., N. Theunissen, S. Zhang, J. Wang, F. Sun, A. A. Ahmed, E. Pihlap, C. T. Reinhard, and N. J. Planavsky (2023), Mitigation of soil nitrous oxide emissions during maize production with basalt amendments, *Frontiers in Climate*, *5*.

Fearnside, P. M., D. A. Lashof, and P. Moura-Costa (2000), Accounting for time in mitigating global warming through land-use change and forestry, *Mitigation and Adaptation Strategies for Global Change*, *5*, 239-270.

Fick, S. E., and R. J. Hijmans (2017), WorldClim 2: new 1km spatial resolution climate surfaces for global land areas *International Journal of Climatology*, *37*, 4302-4315.

Gaillardet, J., D. Calmels, G. Romero-Mujalli, E. Zakharova, and J. Hartmann (2019), Global climate control on carbonate weathering intensity, *Chemical Geology*, *527*.

Goddéris, Y., J. Z. Williams, J. Schott, D. Pollard, and S. L. Brantley (2010), Time evolution of the mineralogical composition of Mississippi Valley loess over the last 10 kyr: Climate and geochemical modeling, *Geochimica et Cosmochimica Acta*, *74*, 6357-6374.

Groom, B., and F. Venmas (2023), The social value of offsets, *Nature*, *619*, 768-773.

Gwiazda, R. H., and W. S. Broecker (1994), The separate and combined effects of temperature, soil pCO2, and organic acidity on silicate weathering in the soil environment: Formulation of a model and results, *Global Biogeochemical Cycles*, *8*, 141-155.

Hamilton, S. K., A. L. Kurzman, C. Arango, L. Jin, and G. P. Rovertson (2007), Evidence for carbon sequestration by agricultural liming, *Global Biogeochemical Cycles*, *21*.

Harrington, K. J., R. G. Hilton, and G. Henderson (2023), Implications of the riverine response to enhanced weathering for CO2 removal in the UK, *Applied Geochemistry*, *152*.

IPCC (2018), Global Warming of 1.5ºC. An IPCC Special Report on the impacts of global warming of 1.5ºC above pre-industrial levels and related global greenhouse gas emission pathways, in the context of strengthening the global response to the threat of climate change, sustainable development, and efforts to eradicate poverty*Rep.*, In press.

Kantola, I. B., et al. (2023), Improved net carbon budgets in the US Midwest through direct measured impacts of enhanced weathering, *Global Change Biology*, *29*, 7012-7028.

Kanzaki, Y., I. Chairavalloti, S. Zhang, N. J. Planavsky, and C. T. Reinhard (2023a), In-silico calculation of soil pH by SCEPTER v1.0, *Geoscientific Model Development*, *In review*, doi:10.5194/gmd-2023-137.

Kanzaki, Y., N. J. Planavsky, and C. T. Reinhard (2023b), New estimates of the storage permanence and ocean co-benefits of enhanced rock weathering, *PNAS Nexus*, *2*.

Kanzaki, Y., S. Zhang, N. J. Planavsky, and C. T. Reinhard (2022), Soil Cycles of Elements simulator for Predicting TERrestrial regulation of greenhouse gases: SCEPTER v0.9, *Geoscientific Model Development*, *15*, 4959-4990.

Knapp, W. J., and E. T. Tipper (2022), The efficacy of enhanced carbonate weathering for carbon dioxide sequestration, *Frontiers in Climate*, *4*.

Kump, L. R., S. L. Brantley, and M. A. Arthur (2000), Chemical weathering, atmospheric CO2, and climate, *Annual Review of Earth and Planetary Sciences*, *28*, 611-667.

Lal, R. (2007), Carbon management in agricultural soils, *Mitigation and Adaptation Strategies for Global Change*, *12*, 303-322.

Larkin, C. S., et al. (2022), Quantification of CO2 removal in a large-scale enhanced weathering field trial on an oil palm plantation in Sabah, Malaysia, *Frontiers in Climate*, *4*.

Lord, N. S., A. Ridgwell, M. C. Thorne, and D. J. Lunt (2015), An impulse response function for the "long tail" of excess atmospheric CO2 in an Earth system model, *Global Biogeochemical Cycles*, *30*, 2-17.

Oh, N.-H., and P. A. Raymond (2006), Contribution of agricultural liming to riverine bicarbonate export and CO2 sequestration in the Ohio River basin, *Global Biogeochemical Cycles*, *20*.

Pan, B., S. K. Lam, E. S. Wang, A. Mosier, and D. Chen (2021), New approach for predicting nitrification and its fraction of N2O emissions in global terrestrial ecosystems, *Environmental Research Letters*, *16*.

Pelletier, J. D., P. D. Broxton, P. Hazenberg, X. Zeng, P. A. Troch, G. Niu, Z. C. Williams, M. A. Brunke, and D. Gochis (2016), Global 1-km gridded thickness of soil, regolith, and sedimentary deposit layers, edited by O. DAAC, Oak Ridge, Tennessee, USA.

Poggio, L., L. M. DeSousa, N. H. Batjes, G. Heuvelink, B. Kempen, E. Ribiero, and D. Rossiter (2021), SoilGrids 2.0: Producing soil information for the globe with quantified spatial uncertainty, *Soil*, *7*, 217-240.

Pumpanen, J., et al. (2004), Comparison of different chamber techniques for measuring soil CO2 flux, *Agricultural and Forest Meteorology*, *123*, 159-176.

Reershemius, T., et al. (2023), Initial validation of a soil-based mass-balance approach for empirical monitoring of enhanced rock weathering rates, *Environmental Science & Technology*, *57*, 19497-19507.

Reershemius, T., and T. J. Suhrhoff (2023), On error, uncertainty, and assumptions in calculating carbon dioxide removal rates by enhanced rock weathering in Kantola et al., 2023, *Global Change Biology*, *30*.

Reitz, M., W. E. Sanford, G. B. Senay, and J. Cazenas (2017), Annual estimates of recharge, quick-flow runoff, and evapotranspiration for the contiguous US using empirical regression equations, *J Am Water Resour As*, *53*, 961-983.

Renforth, P., and G. Henderson (2017), Assessing ocean alkalinity for carbon sequestration, *Reviews of Geophysics*, *55*, 636-674.

Richards, K. R. (1997), The time value of carbon in bottom-up studies, *Critical Reviews in Environmental Science and Technology*, *27*, S279-S292.

Rodell, M., et al. (2004), The Global Land Data Assimilation System, *Bulletin of the American Meteorological Society*, *85*, 381-394.

Rogelj, J., et al. (2018), Scenarios toward limiting global mean temperature increase below 1.5ºC, *Nature Climate Change*, *8*, 325-332.

Smith, S. M., et al. (2023), The State of Carbon Dioxide Removal - 1st Edition*Rep.*

Snaebjörnsdóttir, S. O., B. Sigfússon, C. Marieni, D. Goldberg, S. R. GIslason, and E. H. Oelkers (2020), Carbon dioxide storage through mineral carbonation, *Nature Reviews Earth & Environment*, *1*, 90-102.

Spencer, W. F. (1954), Influence of cation-exchange reactions on retention and availability of cations in sandy soils, *Soil Science*, *77*, 129-136.

Tuanmu, M. N., and W. Jetz (2014), A global 1-km consensus land-cover product for biodiversity and ecosystem modeling, *Global Ecology and Biogeography*, *23*, 1031-1045.

USDA (2011), RCA Appraisal 2011*Rep.*, Washington, DC.

Val Martin, M., et al. (2023), Improving nitrogen cycling in a land surface model (CLM5) to quantify soil N2O, NO, and NH3 emissions from enhanced rock weathering with croplands, *Geoscientific Model Development*, *16*, 5783-5801.

van Kooten, G. C., P. Withey, and C. M. T. Johnston (2021), Climate urgency and the timing of carbon fluxes, *Biomass and Bioenergy*, *151*.

Walkinshaw, M., A. T. O'Geen, and D. E. Beaudette (2022), Soil Properties, California Soil Resource Lab, edited.

Wang, Y., J. Mao, M. Jin, F. M. Hoffman, X. Shi, S. D. Wullschleger, and Y. Dai (2021a), Development of observation-based global multilayer soil moisture products for 1970 to 2016, *Earth System Science Data*, *13*, 4385-4405.

Wang, Y., Z. Yao, Y. Zhan, X. Zheng, M. Zhou, G. Yan, L. Wang, C. Werner, and K. Butterbach-Bahl (2021b), Potential benefits of liming to acid soils on climate change mitigation and food security, *Global Change Biology*, *27*, 2807-2821.

Weihermüller, L., J. Simens, M. Deurer, S. Knoblauch, H. Rupp, A. Göttlein, and T. Pütz (2007), In situ soil water extraction: A review, *Journal of Environmental Quality*, *36*, 1735-1748.

Yasuda, Y., Y. Ohtani, Y. Mizoguchi, T. Nakamura, and H. Miyahara (2007), Development of a CO2 gas analyzer for monitoring soil CO2 concentrations, *Journal of Forest Research*, *13*, 320-325.

Zeng, S., G. Kaufmann, and Z. Liu (2022), Natural and anthropogenic driving forces of carbonate weathering and the related carbon sink flux: a model comparison study at global scale, *Global Biogeochemical Cycles*, *36*.

Zhang, S., N. J. Planavsky, J. A. R. Katchinoff, P. A. Raymond, Y. Kanzaki, T. Reershemius, and C. T. Reinhard (2022), River chemistry constraints on the carbon capture potential of surficial enhanced rock weathering, *Limnology and Oceanography*, doi:10.1001/lno.12244.

Zhao, M., F. A. Heinsch, R. R. Nemani, and S. W. Running (2005), Improvements of the MODIS terrestrial gross and net primary production global data set, *Remote Sensing of Environment*, *95*, 164-176.

TABLES

Table 1. Sources of observational data for model spin-up and tuning.

Parameter	Observational Dataset
Temperature	[*Fick and Hijmans*, 2017]
Soil moisture	[*Wang et al.*, 2021a]
Runoff/infiltration	[*Reitz et al.*, 2017]
Soil pH	[*Poggio et al.*, 2021]
Soil organic matter	[*Poggio et al.*, 2021]
Cation exchange capacity	[*Walkinshaw et al.*, 2022]
Nitrification rate	[*Pan et al.*, 2021]
Base saturation	[*Poggio et al.*, 2021]
Soil erosion	[*USDA*, 2011]
Soil porosity	[*Rodell et al.*, 2004]
Cropland fraction	[*Tuanmu and Jetz*, 2014]
Net primary production (NPP)	[*Zhao et al.*, 2005]

FIGURES:

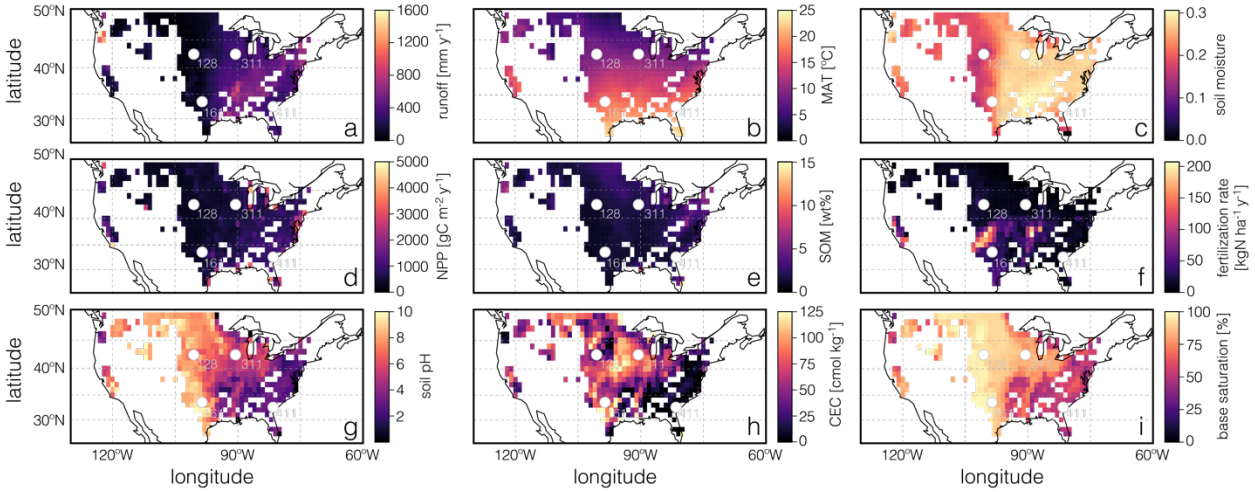

Figure 1. Gridded input data and boundary conditions from the coterminous U.S. used in our reaction-transport model. Key input parameters include runoff (a), mean annual air temperature (MAT; b), soil moisture (c), above ground net primary production (NPP; d), soil organic matter (SOM; e), fertilization rate (f), initial soil pH (g), soil cation exchange capacity (CEC; h), and soil base saturation (i). Also shown are the four site locations discussed in the text (open circles), labelled by site number.

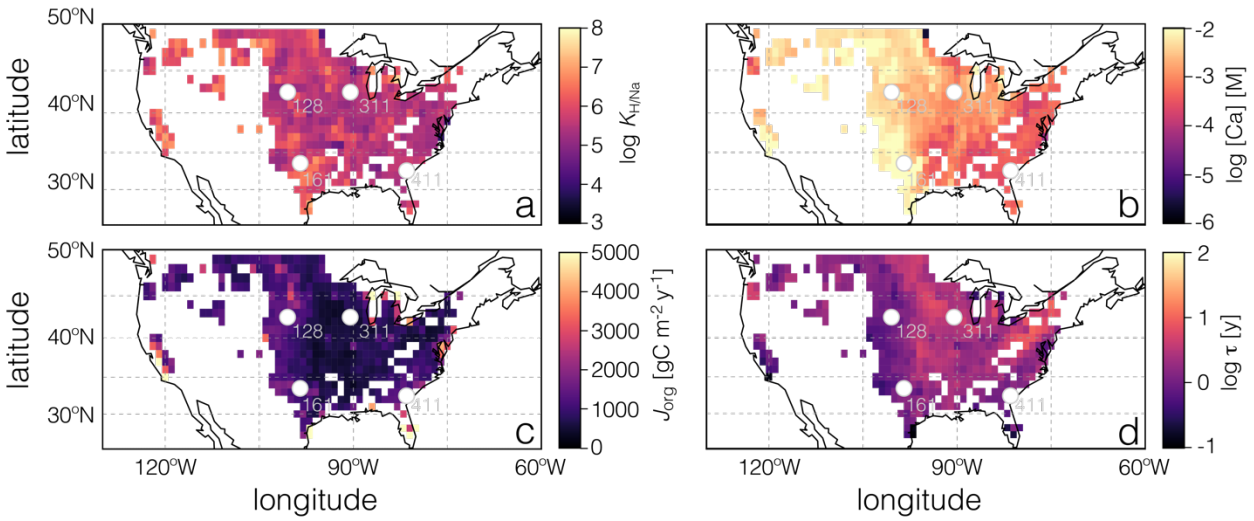

Figure 2. Results for gridded tuned parameters obtained during model spinup. Shown are soil cation exchange cofficients ($K_{H/Na}$; a), soil surface dissolved calcium concentrations ([Ca]; b), organic carbon fluxes to the soil surface (J_{org}; c), and turnover times for soil organic carbon (t; d). Also shown are the four site locations discussed in the text (open circles), labelled by site number.

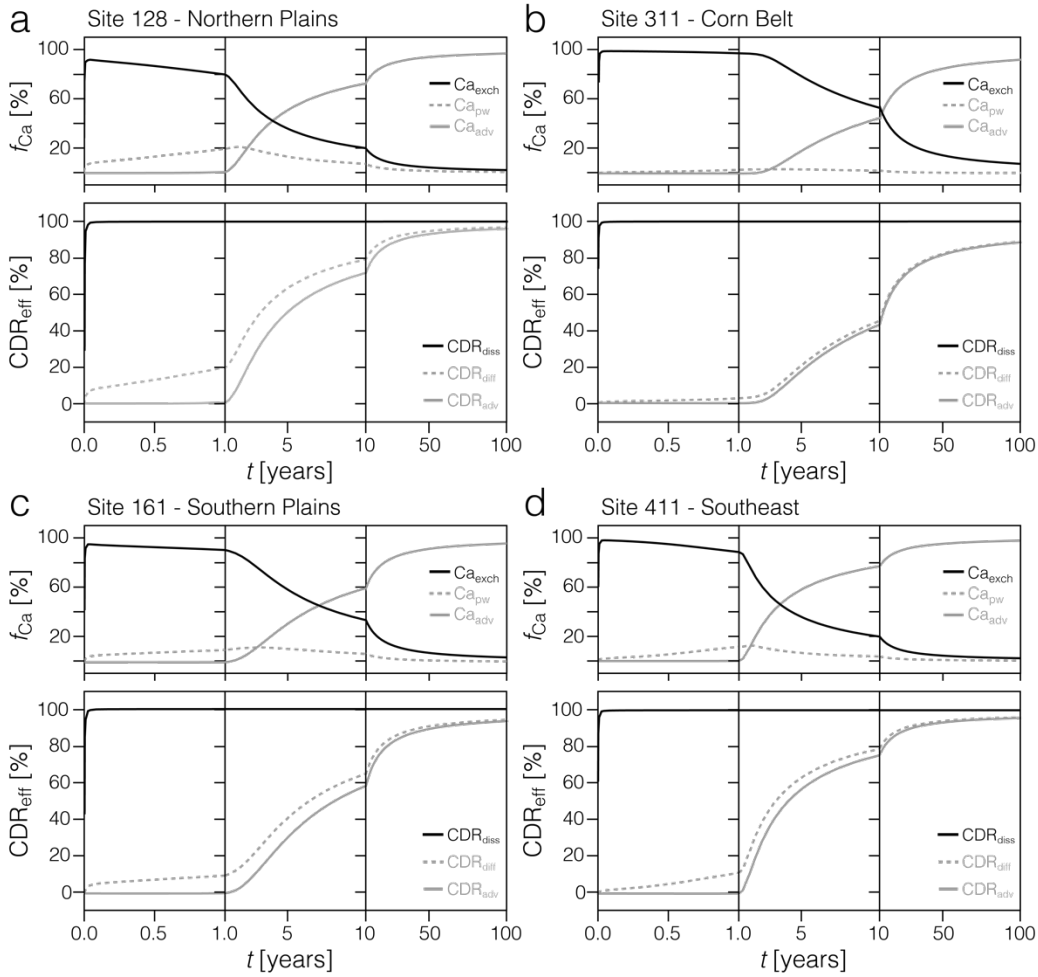

Figure 3. Time-dependent cation and CO_2 removal dynamics for the four sites discussed in the text. The upper panel for each site shows the relative distribution of calcium (Ca), the primary cation tracer in our simulations, between dissolved porewater Ca (Ca_{pw}), exchangeable Ca (Ca_{exch}), and Ca advecting through the soil column (Ca_{adv}). The lower panel for each site shows the carbon dioxide removal efficiency relative to perfect (stoichiometric) removal (CDR_{eff}) according to three CDR metrics — tracking dissolution of the solid phase (CDR_{diss}), tracking changes in soil CO_2 diffusion (CDR_{diff}), and tracking advection of dissolved inorganic carbon (DIC) out of the model domain (CDR_{adv}).

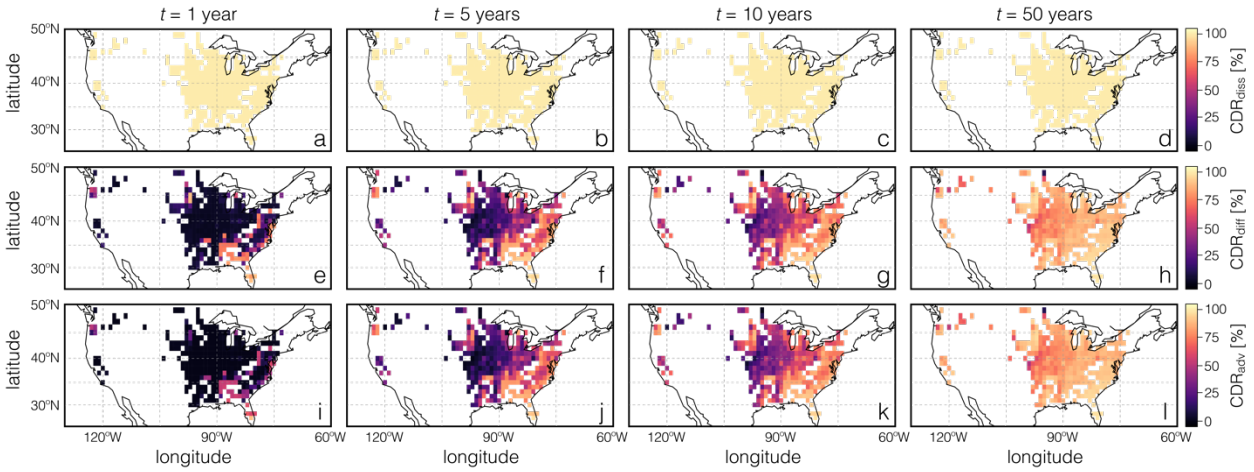

Figure 4. Regional variability in carbon dioxide removal efficiency relative to stoichiometric removal (CDR_{eff}) over time. Shown from left to right are cumulative CDR_{eff} values for time horizons of 1, 5, 10, and 50 years from the start of feedstock application. (a-d) CDR_{eff} values relative to fractional feedstock dissolution (CDR_{diss}); (e-h) CDR_{eff} values relative to changes in soil CO_2 diffusion (CDR_{diff}). (i-l) CDR_{eff} values relative to changes in the advection of dissolved inorganic carbon (DIC) out of the model domain (CDR_{adv}).

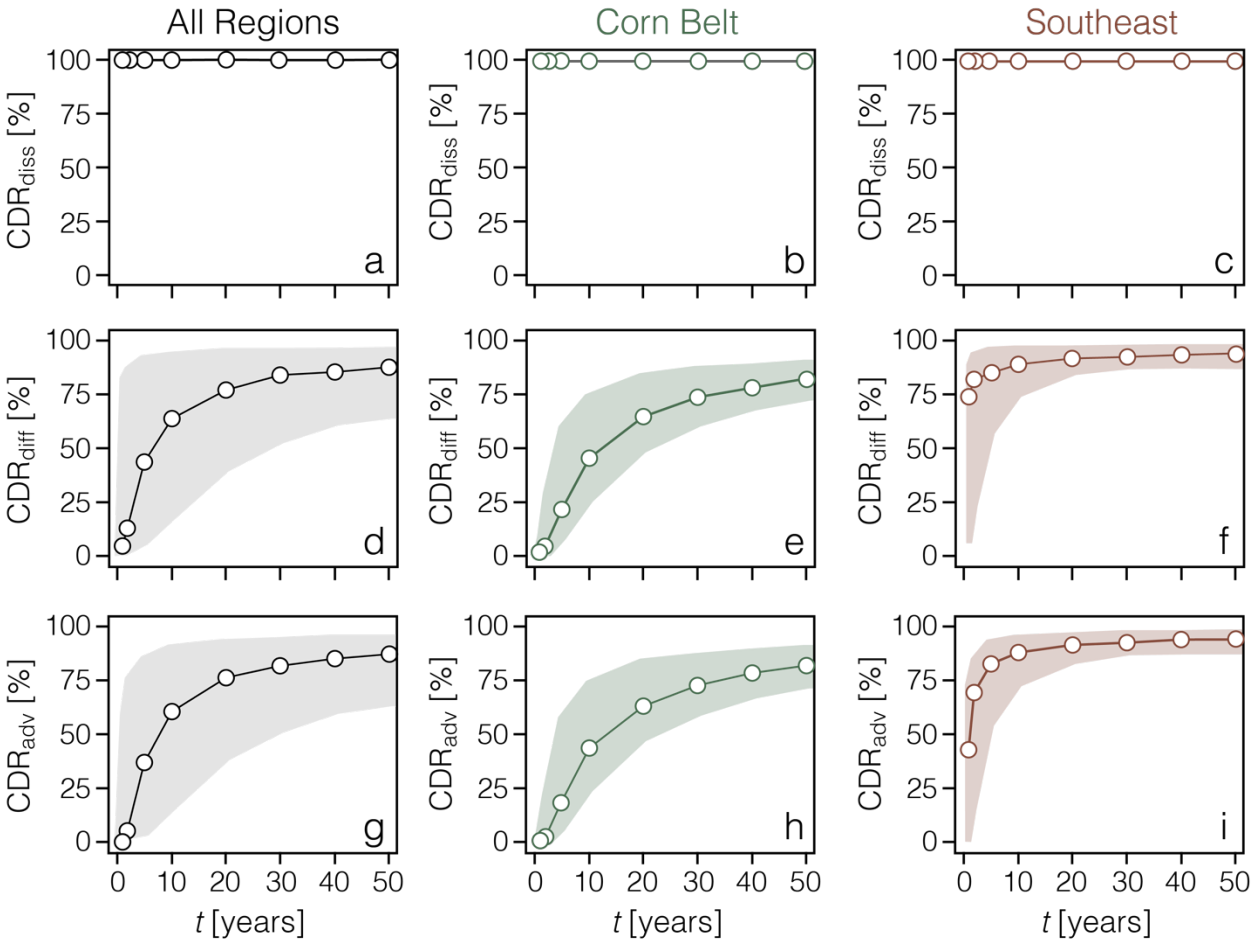

Figure 5. Aggregated regional CDR efficiency (CDR_{eff}) over time. Median values (open circles) and 95% confidence intervals (shaded envelopes) are shown for all U.S. grid cells examined here (left), aggregated Corn Belt grid cells (middle), and aggregated grid cells from the Southeastern U.S. (right). Values are shown relative to solid feedstock dissolution (CDR_{diss}; a-c), changes in soil CO_2 diffusion (CDR_{diff}; d-f), and changes in advection of dissolved inorganic carbon (DIC) out of the model domain (CDR_{adv}; g-i).

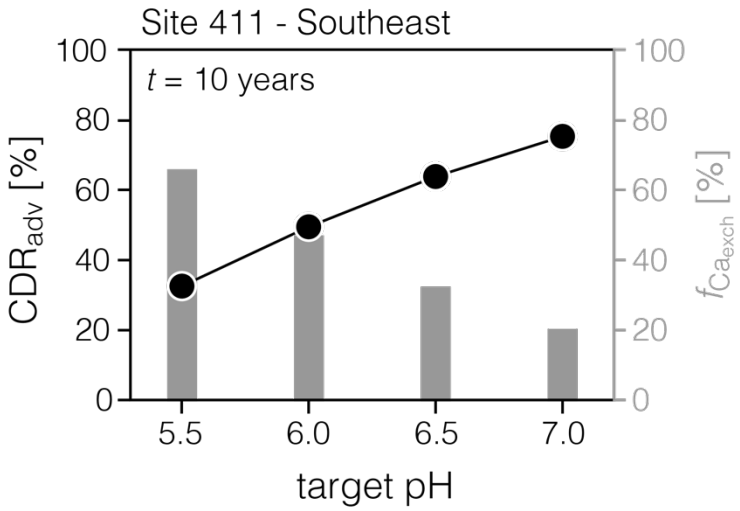

Figure 6. Example simulations from Site 411 (Southeast region) showing the impact of agronomic target pH on the fraction of calcium in the exchangeable pool ($f_{Ca,exch}$) and advective CDR efficiency (CDR_{adv}) over time. All results are shown for a time horizon of 10 years after initial alkalinity modification. Increasing agronomic target pH results in more rapid shift in base saturation of the soil exchange complex, reducing the timescale required to achieve a given CDR efficiency.